A novel linear predictive control approach for auxiliary energy supply to a solar thermal combistorage

Martin Felix Pichler[a,*], Werner Lerch[a], Andreas Heinz[a], Gregor Goertler[b], Hermann Schranzhofer[a], René Rieberer[a]

[a] *Graz University of Technology, Institute of Thermal Engineering, Inffeldgasse 25/B, 8010 Graz, Austria*
[b] *University of Applied Sciences, Campus Pinkafeld, Steinamangerstraße 21, 7423 Pinkafeld, Austria*

Abstract

This paper presents and investigates a novel, hybrid model predictive approach to control the auxiliary heating for a combistorage. Faulty design, as well as suitable design schemes cause situations in which solar energy supply has to "compete against" the auxiliary energy supply. This research demonstrates a feasible method to remedy such situations with the utilization of weather forecast data. The developed approach is modular and expandable to be used with additional heat sources. A suitable disturbance-prediction, which approximates the expected solar energy flux into the storage, in connection with a linear model predictive control (MPC), can prevent the auxiliary system to switch on at an early stage and thus reduce the auxiliary energy demand and keep storage capacity for solar thermal energy supply. Results obtained through simulations for selected months show a reduction of auxiliary energy demand up to 40%, when facilitating this approach for a solar thermal combisystem for a single family house. Monthly solar fractions (F_s) increase by approximately 4 percentage points or 5% with respect to the base case.

Keywords: Solar thermal; auxiliary energy supply; model predictive control; weather forecast

*Corresponding author. Tel.: +43-316-873-7312 Fax: +43-316-873-7305 *E-mail address*: martin.pichler@tugraz.at (Martin Felix Pichler)

1. Introduction

This work suggests and investigates a sophisticated predictive weather data incorporating approach to control the auxiliary heating in a solar thermal combistorage. The aim is to increase solar yields and minimize auxiliary heat demand and thermal storage losses.

The paper describes a new hybrid model predictive control (MPC) approach, discusses relevant controller parameters, and shows the auxiliary energy saving potential compared to a base case control, when applying the MPC approach for a solar thermal (ST) combisystem for a single family house.

Ideally, a predictive controller also incorporates the expected energy demand. However, for this research, prediction refers only to utilization of ideal weather forecast data, i.e. the availability of 100% accurate predictions is assumed.

1.1. Background

Solar thermal systems for domestic hot water (DHW) preparation and space heating (SH) in residential buildings are generally controlled by simple two level controllers which activate ST energy supply and/or auxiliary energy supply into a thermal energy storage (TES). The functioning of two level controllers is based on set- and actual-temperatures, but lacks information on actual or expected solar radiation, which may lead to interference of auxiliary- and solar heat supply in case of a combistorage. This reduces the share of ST energy fed into the TES due to the limited storage capacity. A smart weather forecast data incorporating control concept might be able to compensate this shortcoming and thus increase the solar fractions.

ST systems for residential purposes are mainly designed as bivalent systems for which a second (auxiliary) heat source feeds into the TES. Ideally, the whole TES is exclusively assigned to the ST system. However, design aspects require the ST system to share a certain part of the TES with the auxiliary heat source.

In practice deficient hydraulic schemes often hinder the ST system to contribute a considerable share of the energy supplied to the storage. The guarantee of ST yields comparable to simulation results and practical design in accordance with existing quality standards are still a challenge, especially for small and intermediate plants without monitoring (see Krause, 2003; de Keizer, 2012; Augsten, 2012; Ullrich, 2013). Two level controllers

without any intelligence are not capable to compensate any faulty design, but even for suitable design schemes sometimes the ST system has to "compete against" an auxiliary system in terms of assigned storage capacity.

A predictive weather forecast data utilizing controller might be a remedy to partly compensate for a lacking design as well as to decrease the auxiliary energy fed into the TES. The maximum potential performance enhancement when applying such an approach has already been investigated by Pichler et al. (2012). The *performance bound* indicating the maximum improvement potential is up to 10% for annual solar fractions and up to 30% for a certain month. These results were obtained with the same system as is used in this investigation.

1.2. Energy meteorology and irradiance forecasts

One motivation to facilitate solar irradiance forecasts for the control of a ST plant is the increased frequency and accuracy of these data boosted by the demand for day-ahead and intra-day predictions for solar power plants (see Girodo, 2006; Bacher et al., 2009; Fernandez-Jimenez et al., 2012).

Fig. 1 shows results for the forecast accuracy in Europe. The root-mean-square-error (RMSE) increases only slightly with the forecast horizon, here up to three days ahead. The dashed line *mean of best* indicates the accuracy for cutting edge forecast methods. Forecasts in winter, fall and spring are worse than in summer and the relative RMSE for hourly irradiance data ranges between 40–60% in central Europe. For more details see Perez et al. (2007, 2010); Lorenz et al. (2007); Cebecauer et al. (2010); Wang et al. (2011). Temperature prediction is dealt with in Anadranistakis et al. (2004); Doeswijk (2007); Mathiesen and Kleissl (2011); Richardson et al. (2011).

For this study ideal solar irradiance and temperature forecast data are used, i.e. forecast data facilitated by the MPC match exactly the data during the simulation for testing the approach.

1.3. Predictive control for heating applications

Weather data incorporating predictive control schemes for applications related to heating in buildings, are a promising technology with rising importance. Research activities in this field are growing (e.g. Wimmer, 2004; GÃď hler et al., 2007; BeigelbÃűck, 2009; Lukasse et al., 2009; Gyalistras and Gwerder, 2010; Rovas, 2011). Applied methods are the canonical approach making use of a (linear) model in connection with Quadratic Programming (QP) (e.g. Oldewurtel et al., 2012) and different stochastic approaches using

non-linear simulation models (e.g. Schuss, 2011; Pichler et al., 2011). In general, theoretical studies use ideal weather predictions, i.e. weather data for testing via simulations are the same as those supplied to the predictive controller. Current challenges relate mainly to the modeling (see Sturzenegger et al., 2012).

1.4. Control strategies for residential solar thermal plants

Different control strategies for ST plants may be applied for the pump of the collector loop and for ST heat supply into the TES. In addition, ST combisystems require a suitable control for the auxiliary heat source. Comprehensive optimizations consider also minor mechanical changes to improve the control (see e.g. Krause, 2003). Objectives when optimizing a control task refer to minimization of electricity consumption or monetary costs (see e.g. Ferhatbegovic et al., 2011) and auxiliary energy demand, and/or to maximization of the ST yield; the aim of this research refers to the last two, closely linked aspects.

1.4.1. Review on standard control strategies

The volume of a solar combistorage is typically divided into two main parts. The upper auxiliary volume (V_{aux}, compare Fig. 2) is the part that can either be heated by the auxiliary heating system (usually a boiler) or by solar heat — if available at sufficiently high temperature. The lower part of the storage (V_{solar}) is reserved exclusively for ST heat supply.

In order to enable and maintain thermal stratification, solar charging is often performed with different inlet heights or with a stratification device (see Streicher and Bales, 2005). Increasing V_{solar} and thus decreasing V_{aux} generally results in higher solar fractions (F_s), but V_{aux} cannot be eliminated completely, mainly due to the high thermal power requirements during DHW draw-offs, which cannot solely be covered by the auxiliary source owing to its limited thermal power. Usually V_{aux} is sized such, that a daily DHW demand can be covered, i.e. 200–300 litres for a single family house (SFH) (see Bales et al., 2003).

Charging of V_{aux} by the auxiliary source is usually performed by means of a simple two-level controller, i.e. the decisions related to the charging of V_{aux} are made according to the actual storage temperature. This control approach requires one or two temperature sensors placed in V_{aux}. If only one sensor is being used, it has to be placed low enough to detect discharging of the SH zone — the volume between the SH loop pipe connections, see Fig. 2 —

but the temperature criteria for auxiliary heating (on-signal and off-signal) have to be based on the temperature requirements for DHW (Haller, 2010). If two temperature sensors are being used and placed at different heights, the upper can be used for the on-signal, and the lower for the off-signal. These two sensors are placed in the overlap zone of V_{aux} and the SH zone. Haller reports that this approach outperforms the one sensor approach, both concerning the number of burner starts and the energy savings for a solar combisystem with a pellet boiler. For efficiency measures by minimizing temperatures see ThÃijr (2007).

In this work the base case is the two sensor approach, compare with Fig. 2, and it is assumed that the auxiliary source is switched on when T_{aux1} drops below 57 °C and turns off when T_{aux2} exceeds 63 °C.

1.4.2. Advanced control strategies

The first investigation on sophisticated control strategies for ST systems for residential purposes, known to the authors, has been conducted at the ETH Zurich in the early eighties (see e.g. GrÃijnenfelder and TÃűdtli, 1985). Control strategies incorporating weather forecast data showed to require less auxiliary energy than other simple strategies. An economic MPC has been recently analysed by Halvgaard et al. 2012.

This paper introduces a novel, solar irradiance forecast incorporating linear MPC approach for auxiliary energy supply into the TES. The concept is based on a MPC with a time-invariant *state space model* (SSM) for the TES, and supplementing *mini-simulation results* to be used as future disturbances. Section 2 presents the system description and outlines the used methodologies for investigation of the control approach. Section 3 deals with the MPC approach, describes the required mathematical models starting from first principles, and explains the disturbance generation. Testing and performance indicators are the topics of Section 4, and Section 5 provides results for different scenarios. Section 6 draws a conclusion on the suggested control approach.

2. Methodology

A ST combisystem is designed and simulated in TRNSYS — which is the base case. Consequently a MPC is created in MATLAB, which is embedded in TRNSYS, and employed to control the auxiliary heating in the TES — this is the predictive control approach. This Section outlines the base case

ST system and important boundary conditions, and addresses adaptions for investigation of the suggested predictive control approach. Further, the functioning of the MPC is briefly explained.

2.1. Modeling the ST system

The ST combisystem selected for testing the MPC approach has been configured and extensively used in international research activities on ST systems (see Heimrath and Haller, 2007; Dott et al., 2012). Hence it is possible to compare obtained results for the same climate data against a number of available simulation results with different configurations. Fig. 2 shows the essential elements, in- and outlets and sensors for the investigated ST combisystem. This system has been defined for a single family house with an annual heating energy demand of approximately 45 kWh/m^2 for the climate of Strasbourg. Tab. 3 lists the most important parameter values.

2.2. Simulation data and load profiles

Synthetic climate data and load profiles for a SFH form the main ingredients to obtain simulation results with TRNSYS (Klein et al., 2010), conducted with a time STEP of 1/30 h.

Used climate data for Strasbourg (48.55N 7.63E, heating design temperature = -10 °C, average T_a = 11 °C) were obtained with Meteonorm 6.1.0.9 (see Meteotest, 2009).

In this research the SH and the DHW demand, and the building as such are emulated for the investigation of the combisystem by means of load profiles. The used profiles are those which have been derived for IEA SHC Task 44 for a SFH with an annual heat demand of 45 kWh/m^{2}for the climate Strasbourg, (see Dott et al., 2012, part A, part B). The heating load profile considers occupation and internal gains. The average daily DHW load is 5.84 kWh resulting in 2133 kWh/a for a cold water temperature of 10 °C. The maximum draw off temperature is 55 °C, required by a dish washer.

2.3. Integration of the MPC

System operation in base case mode with a simple two-level controller is represented by Fig. 2. Operation with the sophisticated MPC approach described in this research requires a few adaptions.

2.3.1. Adaptions for MPC operation

Auxiliary heating with the MPC differs from the base case mainly in three aspects:

(i) the controller uses predicted data to determine control actions $\dot{Q}_{aux}$

(ii) the number of required parameters is higher, and

(iii) the auxiliary power is (for now) assumed to be continuously adjustable.

Investigations with the MPC require a replacement of the simple control with T_{aux1} and T_{aux2}, compare Tab. 3.

The most important elements around the MPC controller are drawn in Fig. 3. *Predicted weather data* are forecast data for e.g. the next 12 h. *Actual values* refer to typically available measurement values from the ST system (e.g. storage Temperature at three different heights, collector temperature, etc.). *MPC parameter* stands for the set of parameters required by the MPC (e.g. the maximum auxiliary power, the minimum allowed temperature for the auxiliary part of the TES, etc.). *Reference value* is the target temperature for the auxiliary part of the TES.

2.3.2. The functioning of the MPC

In a nutshell, the MPC controller strives to approximate the reference value by adjusting $\dot{Q}_{aux}$ accordingly, but at the same time it aims to minimize a cost function. That is, the controller has to find a compromise between deviation from the reference value and costs, which is essentially auxiliary energy usage.

To allow for comparison against the base case controller the reference value (set point) temperature must be suitable. In the base case the lowest auxiliary volume temperature results from the rule "on if $T_{aux1} < 57$ °C". Considering stratification this means approximately 60 °C at the top of the storage. Since the model for the TES, as part of the MPC, has a few thermal nodes only, a reasonable "average set point" for the top node, which is close to V_{aux} in size, has to be defined. The defined reference value is 58 °C. [1]

The next Section 3 describes the three elements of the MPC routine in detail: disturbance-prediction, the MPC design, and the SSM — a five node model for the TES.

[1] Ideally the size of the node for which this average set-point (reference value) is set, is exactly the size of the auxiliary volume.

2.4. Simulation with TRNSYS

The base case and the developed MPC approach are tested and investigated with TRNSYS simulations.

Fig. 4 provides a flow chart for this simulation, conducted with a time STEP of 1/30 h. The first gray box indicates the call of the solar combisystem. For *base case* simulations $\dot{Q}_{aux}$ — the auxiliary heater power for V_{aux} — is either $\dot{Q}_{aux,max}$ or zero according to the control rule given in Tab. 3; and the MPC-routine is ignored. In *MPC mode*, $\dot{Q}_{aux}$ is the output from the MPC-routine, which is called at the end of every time STEP, i.e. when intermediate results are convergent.

The MPC-routine is essentially a MATLAB script embedded in TRNSYS via type 155. After some initialization at the very beginning, the routine reads intermediate results from TRNSYS in every time STEP; e.g. the storage temperatures needed for initialization of disturbance-prediction and the MPC. *Disturbance prediction* evoked initially and every 10^{th} STEP, stands for the generation of expected ST energy flux into and inside the TES, originating from predictions of irradiance on the collector field, compare Fig. 6. Consequently the MPC is called, which is essentially the execution of the MPC toolbox function *mpcmove* (see Bemporad et al., 2010, User Manual). This function generates the optimal controller action, which is the auxiliary power for the next time STEP.

3. Predictive control design

This section explains the design of the hybrid MPC approach in detail. A prerequisite for the *linear* MPC is a model for control action evaluation; here it is a model for the thermal storage which is derived in Section 3.1.1. Another vital aspect is the provision of future disturbances. The generation of solar irradiance dependent disturbances from a *non linear* simulation which uses the same model as the MPC is addressed in Section 3.3.

Important aspects and assumptions for this research are:

(i) The controlled variable is the average temperature of the top node of a five node storage — roughly the default auxiliary volume.

(ii) The minimum acceptable value for this variable is constrained due to comfort requirements.

(iii) The "plant" model being part of the MPC is a linear time-invariant state space model (SSM) of the combistorage.

(iv) Disturbance prediction is based on ideal forecast data for solar irradiance and ambient temperature.

(v) DHW draw off and SH demand are *not considered* for disturbance-prediction. In reality DHW draw off is difficult to predict. SH demand could be approximated, but to keep the problem simple at this first stage, it was neglected.

(vi) The controller output must be proportional to power, and the maximum value is given by the maximum power of the auxiliary heater.

(vii) Storage temperatures from the (simulated) ST system are available.

3.1. Linear model predictive control

The canonical MPC problem is formulated in the state space, where the controlled system is described by a linear discrete time model (see Morari and Lee, 1999; Maciejowski, 2002). In terms of noise and disturbances, herein only "measured" disturbance is considered.

$$\begin{aligned} \mathbf{x}(k+1) &= \mathbf{A}\mathbf{x}(k) + \mathbf{B}_u\mathbf{u}(k) + \mathbf{B}_v\mathbf{v}(k) \\ \mathbf{y}(k) &= \mathbf{C}\mathbf{x}(k) \end{aligned} \tag{1}$$

In Eq. (1) $\mathbf{x} \in \mathbb{R}^n$ is the state vector, $\mathbf{u} \in \mathbb{R}^m$ is the control action, $\mathbf{v} \in \mathbb{R}^{\tilde{m}}$ is the disturbance vector, and $\mathbf{y} \in \mathbb{R}^p$ is the (measurable) output vector, with n, m, $\tilde{m}$, $p \in \mathbb{N}$, determining the number of components, respectively. The index k indicates the discrete time instant. $\mathbf{A} \in \mathbb{R}^{n\times n}$, $\mathbf{B}_u \in \mathbb{R}^{n\times m}$, and $\mathbf{B}_v \in \mathbb{R}^{n\times \tilde{m}}$ are the state and the input matrices, and $\mathbf{C} \in \mathbb{R}^{p\times n}$ is the output matrix.

The contextual physical meaning of vectors and matrices from the SSM defined by Eq. (1) is described next.

3.1.1. Thermal storage – state space model (SSM)

In terms of MPC the SSM is used to determine the optimal future control actions (u). In this research, the heating process in the auxiliary volume of the combistorage must be controlled, hence a model for heating this part of the TES is required. In principal, $T_{S1} = f(\dot{Q}_{dis,S1}, V_{aux})$ can be approximated by a PT1 characteristic (compare Halvgaard et al., 2012), when assuming adiabatic boundary conditions for V_{aux}, but in connection with an open collector loop an acceptable prediction accuracy of only 1-2 hours is obtained, which is too low. The reason is, that the open loop does not notice temperature increases in the lower part of the storage.

The linear time-invariant SSM derived for the MPC in this work, is a five node model for the combistorage, where each node corresponds to one state. State changes due to internal mixing between nodes, are modeled in $\mathbf{A}$. Auxiliary energy input via $\mathbf{u}$ is considered through $\mathbf{B}_u$, and a priori disturbances $\mathbf{v}$ are incorporated via $\mathbf{B}_v$. $\mathbf{C}$ maps the internal states (node-temperatures) on the output vector $\mathbf{y}$ representing the measurable outputs.

Starting from first principles the physical interactions of a thermal node i to the node above and below and to the ambient are given by Eq. (2a–c). Eq. (2) summarizes the energy balance for the i-th node, where $\dot{Q}_{aux,Si}$ and $\dot{Q}_{dis,Si}$ stand for auxiliary energy flux, and disturbance energy flux originating from solar energy input. This energy balance holds for each node but $\dot{Q}_{c,i+1}/\dot{Q}_{c,i-1}$ is zero for the top/bottom node.

$$\dot{Q}_{c,i+1} = UA_{i+1}(T_{Si+1} - T_{Si}) \tag{2a}$$

$$\dot{Q}_{c,i-1} = UA_{i-1}(T_{Si-1} - T_{Si}) \tag{2b}$$

$$\dot{Q}_{a,i} = UA_{a,i}(T_{Sa} - T_{Si}) \tag{2c}$$

$$m_i c_p \frac{dT_{Si}}{dt} = \dot{Q}_{c,i+1} + \dot{Q}_{c,i-1} + \dot{Q}_{a,i} + \dot{Q}_{aux,Si} + \dot{Q}_{dis,Si} \tag{2}$$

Although a five node SSM is used later, only three nodes are assumed for demonstration. The state vector represents the storage node temperatures

$$\mathbf{x} \;:=\; [T_{S1}, T_{S2}, T_{S3}]^T. \tag{3}$$

The control actions ($\mathbf{u}$) are auxiliary energy flux. The disturbances ($\mathbf{v}$) represent the ST-induced energy flux to the storage nodes and the storage ambient temperature.

$$\mathbf{u} \;:=\; [\underbrace{\dot{q}_{aux,S1}}_{=:\dot{q}_{aux}}, \underbrace{\dot{q}_{aux,S2}, \dot{q}_{aux,S3}}_{=0}]^T, \tag{4}$$

$$\mathbf{v} \;:=\; [\dot{q}_{dis,S1}, \dot{q}_{dis,S2}, \dot{q}_{dis,S3}, T_a]^T\,, \tag{5}$$

where

$$\dot{q}_{aux,Si} = \frac{\dot{Q}_{aux,Si}}{m_n c_p}\,, \quad \dot{q}_{dis,Si} = \frac{\dot{Q}_{dis,Si}}{m_n c_p}\,, \tag{6}$$

stand for normalized auxiliary and disturbance energy flux in K/h, respectively. Normalized power is a measure for the temperature change per hour,

which is obtained when supplying e.g. $\dot{Q}_{aux,Si}$ to a thermal node with mass m_n and specific heat capacity c_p. For the given control task auxiliary power is supplied to the top node only, hence the other components of $\mathbf{u}$ are zero.

Writing the energy balance from Eq. (2) for each node and using the definitions from Eq. (3–6), after dividing by $m_n c_p$ the following three equations are obtained — assuming equal UA values for internal mixing and the same coefficients for losses against ambient temperature at the top and the bottom.

$$\begin{aligned}
\frac{dx_1}{dt} &= \frac{1}{m_n c_p}\left[-UA - UA_{a,c}, UA, 0\right] \cdot \mathbf{x} + [1,0,0] \cdot \mathbf{u} + [1,0,0, UA_{a,c}/m_n c_p] \cdot \mathbf{v} \\
\frac{dx_2}{dt} &= \frac{1}{m_n c_p}\left[UA, -2UA - UA_{a,m}, UA\right] \cdot \mathbf{x} + [0,1,0] \cdot \mathbf{u} + [0,1,0, UA_{a,m}/m_n c_p] \cdot \mathbf{v} \\
\frac{dx_3}{dt} &= \frac{1}{m_n c_p}\left[0, UA, -UA - UA_{a,c}\right] \cdot \mathbf{x} + [0,0,1] \cdot \mathbf{u} + [0,0,1, UA_{a,c}/m_n c_p] \cdot \mathbf{v}
\end{aligned} \tag{7}$$

$$\Longleftrightarrow \frac{d\mathbf{x}}{dt} = \mathcal{A}\mathbf{x} + \mathcal{B}_u\mathbf{u} + \mathcal{B}_v\mathbf{v}. \tag{8}$$

The matrices $\mathcal{A}$, $\mathcal{B}_u$ and $\mathcal{B}_v$ are obtained by comparing Eq. (7) and Eq. (8) which is the continuous-time counterpart of Eq. (1). Discretization with the according sampling time leads to the matrices $\mathbf{A}$, $\mathbf{B}_u$ and $\mathbf{B}_v$. The output matrix for one measurable output reads

$$\mathcal{C} \equiv \mathbf{C} = \begin{bmatrix} 1 & 0 & 0 \end{bmatrix}. \tag{9}$$

The five node storage SSM matrices, used for the MPC approach to test it within a TRNSYS simulation, are given in Appendix A, Table 4 provides the physical values assigned to the appearing variables. A temperature increase of a node i is possible through auxiliary energy flux $\dot{q}_{aux,Si}$ (only for the top node), or a disturbance $\dot{q}_{dis,Si}$ originating from (expected) ST energy flux. The physical interaction between nodes is reduced to heat conduction; heating due to internal mass flow is hidden in the disturbances, as is the interaction with ambient. To verify the adequacy of this SSM, the five node temperatures were compared against TRNSYS simulation results obtained with the storage type 340 (DrÃijck, 2006), applying a non-uniform thermal charging and discharging cycle over 10 days respectively. The most important

is the accuracy of the top node which proved very good ($\Delta T_{S,top} = 1 \pm 1$ K). Towards the bottom node the deviation of the temperatures increases ($\Delta T_{S,bot} = 1.6 \pm 5$ K). It must be noticed, that this accuracy refers to the MPC model only, not to the storage model that is used later to test the MPC approach.

3.1.2. Optimization problem

Control actions for each discrete time instant are obtained by continuously solving the following open-loop optimization problem — a *Quadratic Programming* (QP) problem.[2] The *cost function* of an MPC problem with one control action and one controlled variable is [3]

$$J_{P,M} = \min_{\Delta u(k|k),\ldots,\Delta u(k+M-1|k),\epsilon} \sum_{i=0}^{P-1} \left(J_{i+1}^{y} + J_{i}^{u} + J_{i}^{\Delta u} + \rho_\epsilon \epsilon^2 \right) \tag{10}$$

where the according terms [4]

$$J_i^y = \left(w^y \left| y(k+i\,|k) - y_{ref}(k+i) \right| \right)^2, \tag{10a}$$

$$J_i^u = \left(w^u \left| u(k+i\,|k) - u_{ref}(k+i) \right| \right)^2, \tag{10b}$$

$$J_i^{\Delta u} = \left(w^{\Delta u} \left| \Delta u(k+i\,|k) \right| \right)^2 \tag{10c}$$

stand for the costs due to deviation of y and u from a reference value, and due to control action increments. All weights (w) in this work are assumed constant. The term $\rho_\epsilon \epsilon^2$ in Eq. (10), expresses the costs due to the maximum required relaxation to fulfil each of the following constraints:

$$\begin{aligned}
& y_{min} - \epsilon V_{min}^{y} \le y(k+i+1\,|k) \le y_{max} + \epsilon V_{max}^{y} \\
& u_{min} - \epsilon V_{min}^{u} \le u(k+i\,|k) \le u_{max} + \epsilon V_{max}^{u} \\
& \Delta u_{min} - \epsilon V_{min}^{\Delta u} \le \Delta u(k+i\,|k) \le \Delta u_{max} + \epsilon V_{max}^{\Delta u} \\
& \Delta u(k+i\,|k) = 0 \quad \text{if } i \ge M \\
& \epsilon \ge 0, \\
& \text{where } i \in \{0, 1, \ldots, P-2, P-1\}\,.
\end{aligned} \tag{10d}$$

[2] For solving this QP problem standard algorithms are available, for more details see Maciejowski (2002) or Bemporad et al. (2010).

[3] Referring to the SSM from Eq. (1) only the first components of $\mathbf{u}$ and $\mathbf{y}$ are relevant.

[4] In $(k+i\,|\,k)$, the k right to the line indicates the current instant, $k+i$ stands for the absolute sample number; since only i increases during each minimization, the notation in brackets can be understood as "related to the current instant k, i steps ahead".

Given the time-invariant SSM from Eq. (1) and disturbances $\mathbf{v}(k+i)$ for the prediction horizon P $\in \mathbb{N}$, i.e. for $i = 0, 1, \ldots$ P-1; based on the current state $\mathbf{x}$(k) the optimal sequence $\Delta u(k\,|k), \ldots, \Delta u(k+M-1\,|k)$ is found through minimization of $J_{P,M}$, for which the slack variable ϵ provides a way to soften the constraints from (10d). Fig. 5 illustrates the control actions resulting from an optimal sequence of Δu. However, only u$(k|k)$ is really applied, since in the next instant $k+1$ a new optimal sequence and new u's are calculated.[5]

3.2. Specific MPC problem

This section approaches the MPC formulation from a practical point of view, which occasionally results in inexactness. Table 5 describes the role, and provides an intuitive abbreviation related to the physical meaning of each parameter and variable being part of the cost function in Eq. (10), or the constraints (10d). All reference values in this work are assumed constant.

For the given control task, the controlled variable y is the temperature of the storage top node (T_{S1}) and the control action u corresponds to auxiliary power supply ($\dot{q}_{aux}$) to this node. Using the default values from Table 5 and omitting the constraints and the costs due to control action increments for a moment, the cost function for the given MPC task reads

$$J_{36,15} = \min_{\dot{q}^*_{aux}(0),\cdots,\dot{q}^*_{aux}(14)} \sum_{i=0}^{35} \left(T^*_{S1}(i) - 58\right)^2 + \left(w^{\dot{q}_{aux}} \dot{q}^*_{aux}(i)\right)^2 . \qquad (11)$$

This cost function[6] is minimized when the MPC is called, i.e. in every STEP of the outer loop in Fig. 4. The optimal sequence of control actions comprises 15 values for $\dot{q}^*_{aux}$, which are found by means of the SSM for the thermal storage for disturbances $\mathbf{v}$, provided for the prediction horizon of 36 samples. The term $\left(T^*_{S1}(i) - 58\right)^2$ are the costs due to deviation of the temperatures $T^*_{S1}(i)$ from the reference value 58 °C. The term $\left(w^{\dot{q}_{aux}} \dot{q}^*_{aux}(i)\right)^2$ expresses costs for auxiliary energy consumption, for which $w^{\dot{q}_{aux}}$ provides

[5] It has to be noted, that in case of an infeasible solution at instant $k+1$, $\Delta u(k+1|k)$ would be used. Infeasible solutions can be avoided through flexible constraints via the slack variable, which requires relaxation constants $\neq 0$ if possible.

[6] Except for neglected costs due to control action increments, this simplified cost function holds as long as none of the constraints is violated.

flexibility to adjust the relative importance of this cost term. After each successful minimization of Eq. (11), only the first value of the optimal sequence $\dot{q}^*_{aux}(0)$ is really applied for the ST combisystem.

3.3. Disturbance modeling

Disturbance-prediction is the main feature that distinguishes the MPC approach from a simple controller. A priori disturbances represent an estimation for expected ST-induced energy flux into and inside the TES, and the ambient temperature (last component). Solar radiation and ambient temperature forecast data are used to continuously update these data. DHW draw off and SH demand prediction are not considered in this research.

Knowing future ST energy supply into the TES enables the controller to adjust a sufficient but moderate temperature for the auxiliary volume, rather than the maximum set point.

The transformation of predicted solar radiation into disturbances ($\dot{q}_{dis,S1}, \ldots, \dot{q}_{dis,S5}$) is realized by a *mini-simulation* of the solar loop. The complete disturbance vector $\mathbf{v}$, predicted for $i = 1, \ldots, \mathrm{P}$ samples is utilized by the MPC to estimate the future temperature changes in the combistorage, by means of the SSM which was described before.

Mini-simulation for disturbance-prediction

In principal, the required disturbance generation can be conducted with any thermal simulation software such as TRNSYS. However, these software often lacks a possibility to set initial conditions for thermal models compare (Coffey et al., 2010). Hence a MATLAB script for conducting the mini-simulation was set up.

Fig. 6 outlines the flow chart of this simulation. After data preprocessing and initialization, the models of the mini-simulation (light gray boxes) are called one after the other during each sampling interval, until disturbance values are collected for the whole prediction horizon P.

The *collector* model uses an efficiency curve approach, (see Duffie and Beckman, 2006; Kaltschmitt et al., 2007). *Hot* and cold *pipes* are modeled with a plug flow approach. For modeling the *heat exchanger* the effectiveness-NTU method is used. Stratified charging of the TES is determined by the output temperature of the heat exchanger indicated as $T_{solar,in}$ in Fig. 2, the current storage temperatures, and $\dot{m}$. Outputs of *charge* ($\dot{q}_{dis,Si}$) indicate the energy flux in each node, occurring during the charging process. These energy fluxes and the ambient temperature are the *a priori disturbances* to

be used by the MPC controller. Appendix B briefly describes the respective models.

The thermal *storage* plays an important role in the mini-simulation. The bottom node temperature indicated as $T_{S,low}$ in Fig. 2 is needed to obtain the outlet temperature of the solar heat exchanger on the collector loop side. The used model is the five-node storage also applied for the MPC, which was described in Section 3.1.1. In case of temperature inversion, that is $T_{Si+1} > T_{Si}$, the according bordering nodes are set to their average temperature.

A weakness of this approach is the fact that predicted disturbances derived from pure ST stratified charging do not consider auxiliary energy input, which might change the stratification. The alignment of the mini-simulation TES model in every time STEP when it is called, reduces this weakness.

4. Testing and performance indicators

This section defines criteria, used to compare the performance of different MPC scenarios, both against each other and related to the base case. The simulation results used in these definitions are obtained from TRNSYS simulations according to Fig. 4 with a time STEP of 1/30 h, the thermal models of that simulation are much more elaborate than the models used for the mini-simulation.

4.1. Plant performance indicators

Solar fractions (F_s) for N considered simulation values, i.e. $t_i = t_1, t_2, \cdots, t_N$, are calculated according to Eq. (12). $\dot{Q}_{hx}$ and $\dot{Q}_{aux,S1}$ are direct simulation results. The penalty term $\dot{Q}_{pen,lin}$ is the linear part of Eq. (14) and it is considered for the calculation of F_s to compensate for auxiliary energy not included in $\dot{Q}_{aux,S1}$ but needed to fulfill the comfort requirements.

$$F_s \;=\; \frac{\sum_{i=1}^{N} \dot{Q}_{hx}(t_i)}{\sum_{i=1}^{N} \dot{Q}_{hx}(t_i) + \dot{Q}_{aux,S1}(t_i) + \dot{Q}_{pen,lin}(t_i)} \,. \tag{12}$$

The performance change of a ST system for different control strategies is defined by

$$\Delta f_s \;:=\; \frac{(F_{s,mpc} - F_{s,base})/F_{s,base}}{(V_S - V_{aux})/V_S} \,. \tag{13}$$

The nominator is the relative change of F_s, the denominator gives the relative solar volume. Fig. 13 depicts the theoretical performance bound for Δf_s.

4.2. Penalty functions

To allow for comparison of MPC controllers (with different parameters) among each other and against the base case controller, a reasonable penalty function characterising the deviation from a desired set point for e.g. the DHW draw off temperature, is crucial. Therefore the following function is defined (compare Bales et al., 2003).

$$\begin{aligned} \dot{Q}_{pen}(t_i) &:= \dot{m}(t_i)\, c_p\, (\Delta T_{lin}(t_i) + b\, \Delta T_{pow}(t_i)^x) \\ \text{where } \Delta T_{lin}(t_i) &:= \max\left(T_{set}(t_i) - T_{act}(t_i), 0\right), \\ \text{and } \Delta T_{pow}(t_i) &:= \max\left(45\ ^\circ C - T_{act}(t_i), 0\right) \end{aligned} \tag{14}$$

The linear term compensates the energy per time STEP to meet the desired temperature value, and the power function penalizes comfort violations. The variables $\dot{m}$ and c_p are the respective mass flow rate and the specific heat capacity of water. Fig. 7 shows the penalty function for DHW.

4.2.1. DHW discomfort and penalties

Herrmann et al. (1994) conducted an empirical experiment on thermal sensation for humans under showers in France. Results indicate a mean preferred water temperature of 36.3±0.15 °C and a mean thermoneutral temperature of 35.1±0.14 °C. The thermal sensitivity threshold found is 0.6±0.1 K, and discomfort thresholds when starting from preferred conditions are ±(2.4±0.3) K. It has to be noted, that in general the preferred conditions vary individually and especially for different continents.

Based on these findings parameters for Eq. (14) are set b=8, and x=4. This choice leads to the following properties, depicted also in Fig. 7. For temperature deviations below the sensitivity threshold only energy demand is compensated, up to 1.5 K penalties are moderate, but above 1.5 K they are high. The temperature $T_{set}(t_i)$ is the draw off set-temperature, i.e. penalties are calculated from the deviation of the actual draw off temperature $T_{act}(t_i)$ against the planned value, mostly 45 °C. With 45 °C being the baseline a ΔT of approximately 10 K with respect to the preferred water temperature is assured — to account for thermal distribution and transfer losses. E.g. a $\Delta T_{pen}(t_i)$ of 1.5 K at the i-th time STEP (2 min) leads to a penalty of 0.42 kWh, and a $\Delta T_{pen}(t_i)$ of 3 K results in a penalty of 6 kWh, equivalent to 7% and 103%, of the daily DHW energy demand for the SFH (5.84 kWh), respectively.

4.2.2. SH discomfort and penalties

The SH heat demand is obtained from a load profile, hence flow- and return-temperature of this sink are fixed in each time STEP t_i. Since the SH outlet pipe is located in the upper part of the storage, which is already monitored in terms of DHW penalties, and because the SH flow temperature (35 °C) is clearly below the minimum set-value for DHW preparation the penalty function for SH comprises only the linear term in Eq. (14) and $b = 0$.

5. Results and discussion

A number of parameters have to be set for the MPC controller. For few of them rules of thumb can be applied. Some parameters, especially constraints can be derived from physical plant properties or practical considerations, e.g. minimum temperature due to comfort constraints. Finally, simulations are required to find suitable ranges for some MPC parameters of the cost function from Eq. (10), and to evaluate the suggested control approach for different scenarios. Parameters not given explicitly have their default value from Tab. 5, (see also Bemporad et al., 2010, User Manual).

5.1. Characteristic controller behaviour

The control task in this research affords special attention on the following cost function parameters:

(i) $w^{T_{S1}}$, which declares the "importance" of adjusting the reference value $T_{S1,ref}$, This weight is kept constant at 1.

(ii) $w^{\dot{q}_{aux}}$, which declares the "price" for auxiliary energy in the cost function, since the according reference value is zero. This weight is varied.

(iii) P the prediction horizon, which is also investigated.

The assumption of realistic limit cases allows for detection of appropriate parameter values through parameter variation. Hence, simulations for a number of scenarios are conducted. First for pure DHW load (scenario I–III), and second, for DHW and SH load (scenario I–III winter). This is important, since load prediction is not considered herein for now, and different load patterns will lead to different suitable parameter ranges.

5.1.1. Pure DHW load

The following three scenarios assume an initial uniform storage temperature of 30 °C at midnight, 00:00 h. The simulation interval is 24 h and for each scenario the evaluation is based on the following *two criteria*:

(i) $T_{S1,min}$ (45 °C) must be approached with maximum auxiliary power ($\dot{q}_{aux,max}$) and sustained thereafter, and

(ii) a clear trend of T_{S1} towards $T_{S1,ref}$ (58 °C) should be visible; ideally the reference value is approximated within acceptable delay.

In addition, the penalties according to Eq. (14) serve as a useful criteria to identify critical operation conditions. It is assumed for now, that the cumulated penalties for one day must not increase the *critical threshold* of 0.3 kWh/d (5% with respect to the daily consumption).

Scenario I

Assume prediction of an *overcast* day, $I_{C,max} \approx 170$ W/m^2, i.e. the disturbances (ST induced energy supply to the storage) are negligible. Fig. 8 shows the evolution for the mean temperature in the auxiliary part of the storage (a) and the corresponding controller outputs (b) responsible for these temperatures. The four curves correspond to four weights ($w^{\dot{q}_{aux}}$), which value the use of auxiliary power differently. A high weight clearly misses the aim to approximate $T_{S1,ref}$. In any case the penalties are less than the critical threshold. The suitable range for the weights, in light of the two criteria from above, is $w^{\dot{q}_{aux}} = 0, \cdots, 4$.

Scenario II

For a *partly cloudy* day, $I_{C,max} \approx 400$ W/m^2, the temperature curves and the controller behaviour are very similar to scenario I, but the controller output is slightly restrained in the first 12 hours. The second half of the interval is characterised by a clearly visible temperature increase not originating from auxiliary power, but from the disturbance, i.e. ST power supplied into the top node. For this scenario no graphs are shown, but the disturbance looks very similar as for the scenario II winter see Fig. 9 (b). In any case the penalties are below 1.3%. The suitable parameter range found for this scenario is $w^{\dot{q}_{aux}} = 0, \cdots, 5$.

Scenario III

Prediction of a *sunny* day, $I_{C,max} \approx 1000$ W/m^2, leads to similar results as for scenario I and II, but as the sliding prediction window detects the high foresighted disturbance through ST power, the controller output is reduced to zero. In any case the penalties are below 0.1%. It seems the whole range of weights is acceptable. However, the draw off at the beginning of the eight hour might be critical and suggests the parameter range $w^{\dot{q}_{aux}} = 0, \cdots, 3$.

No graphs are shown for this scenario, but the critical instant is also visible for the scenario III winter in Fig. 10(a).

5.1.2. DHW and SH load

In the following, the scenarios I-III are repeated for winter, that is, the total load is given by the sum of the DHW and the SH load profile. The evaluation criteria are the same as for pure DHW load.

Scenario I winter

The additional SH load requires more auxiliary heating, leading to a more diversified controller action compared to Fig. 8. For high weights (10, 4), the aim to sustain T_{S1} at the minimum level (45 °C), is missed in the first half of the simulated interval. A critical situation for a medium weight ($\tilde{4}$) occurs at the seventh hour. Although no graphs are shown for this scenario, a similar critical instant is visible in Fig. 9 (b). The reference value is approximated for low weights only. A parameter range of $w^{\dot{q}_{aux}}$ from 0, $\cdots$, 2.5 prevents from high penalties.

Scenario II winter

The control characteristic for the partly cloudy day in winter differs from the overcast day due to the significant disturbance between the ninth and the 14^{th} hour. Fig. 9 shows the resulting proactive controller behavior; the MPC restrains auxiliary heating in the first half of the simulation interval. A parameter range of $w^{\dot{q}_{aux}}$ from 0, $\cdots$, 3 prevents from high penalties.

Scenario III winter

The curves in Fig. 10 indicate a critical but characteristic situation for MPC operation. The expected high solar radiation during the day leads to stronger restriction of $\dot{q}_{aux}$ in the first 12 h compared to Fig. 9; from the ninth hour on we have pure ST heating. The reduced auxiliary heating as a consequence of the predicted ST power results in a critical operating point at the seventh hour. Although initially a trend to approximate the reference value is clearly visible, as the prediction horizon captures the strong disturbance, the deviation to the reference value increases. This holds even for $w^{\dot{q}_{aux}} = 0$. The results are not alarming in terms of the penalties, since the mean temperature of the node T_{S1} is not the same as the real draw off temperatures and obviously these temperatures do not deviate too much. The suitable range for $w^{\dot{q}_{aux}}$ is 0, $\cdots$, 2.5.

5.1.3. Variation of the prediction horizon (P)

For this investigation the scenarios are the same as for scenario III winter, but the initial storage temperature of 30 °C is assumed around sun set. This way the time span to the next possible sunny period is maximized, which enables to see the difference between a short and a long P.

Scenario IV-P12, P = 12

Compared to all former scenarios, due to the initial storage temperature of 30 °C at around sun set, the START of the simulation interval is 18:00 rather than 00:00. This scenario represents the short prediction horizon. Fig. 11 shows the curves for T_{S1}. The zero weight curve initially approximates the reference value, but as the prediction horizon captures the strong disturbance, the deviation to $T_{S1,ref}$ increases.

Scenario IV-P24, P = 24 h

Scenario IV-P24 with results in Fig. 12 represents the long prediction horizon. Compared to Fig. 11, the strong disturbance is captured earlier, and hence the deviation to the reference value is much higher during the first half of the interval, for $w^{\dot{q}_{aux}}$ is 0, 2 or 4. For $w^{\dot{q}_{aux}} = 0$; the temperature does not even get close to the reference value in the beginning of the simulation interval, whereas for P = 12 h it is approximated for the first seven hours of the interval. Although not analysed explicitly, the characteristic behaviour indicates a higher likelihood for critical situations as P increases. The reason is, that for a small P intervals with no disturbance at all are more likely, and during these intervals the auxiliary volume is heated up close to the reference value.

5.2. Results for longer simulation periods

Investigations on the performance bound show a high theoretical potential for the months March, April and October (compare Pichler et al., 2012). Therefore extended simulations fore these months were conducted with $w^{\dot{q}_{aux}}$ = 2.5 and P = 12. The smaller prediction horizon was chosen because it reduces the likelihood of critical situations in terms of comfort.

Results related to MPC-attributed improvements consider always the linear penalty correction such as in the denominator of Eq. (12), that is any positive effect is purely due to the MPC approach.

Tab. 6 lists the differences for solar fractions between the MPC and the base case, for two different auxiliary volumes. The MPC approach clearly

shows its strength for April and October. For these months, except for Oct. and $V_{aux} = 300$ L, the results are significant and no additional penalties occur during MPC operation. The maximum absolute increase of F_s is approximately 4 percentage points (pp) or 5%.

Fig. 13 shows a performance bound (PB), which is an utterly edge with respect to the theoretical annual improvement potential. The black circles show the improvement potential for the investigated months.

Improvements originate mainly from reduced storage losses which are $-4 \pm 3\%$ when averaging values from the three months for $V_{aux} = 300$ L. The reduced losses are due to lower average storage temperatures; on average $-5 \pm 4\%$ in the top node of the TES and $-2 \pm 1\%$ in the node below. The increase of the *solar input* due to virtually extended solar volume (V_{solar}) is on average $+2 \pm 1\%$. All numbers are with respect to the base case. For $V_{aux} = 500$ L values for average losses and temperatures are approximately one additional percentage point reduced and the increase of the solar input is +3% instead of +2%.

Auxiliary energy savings

Fig. 14 and 15 show the auxiliary energy savings — already corrected by any linear penalties, which may distore the objectivity of the results — for the investigated months when deploying the MPC, compared to the base case, in kWh and in %. The absolute values are very similar, for the relative savings April stands out due to the decreased absolute auxiliary demand for this month. The difference for altered V_{aux} is visbile but not high.

Penalties

The DHW penalties are very progressive for increasing temperature deviations from the draw off set-point, compare with Fig. 7. As was indicated in Table 6 with *Italic numbers* for March and October and especially for $V_{aux} = 300$ L penalties for MPC operation are an issue. The highest cumulated linear penalty for the period of one month is approximately 1.5 kWh, considering the three investigated months. The maximum cumulated value for non-linear penalties is at the order of 10^3 kWh. This is very high, however, e.g. in April no penalties occur at all. These findings and insight from simulations for certain days from other months with high SH demand indicate the importance of further parameter tuning to enable a reliable MPC operation on an annual basis. Even for the base case certain days in January and December with unexpected high penalties were found.

Increasing the minimum set temperature or especially incorporating the SH demand prediction might provide a remedy for this.

5.3. Features of the proposed MPC approach

Existing MPC solutions in the context of residential heating are either focusing mainly only on the building (Oldewurtel et al., 2012; Privaraa et al., 2013) or are tailored to one special control task (Wimmer, 2004; Bianchi, 2006; Halvgaard et al., 2012). Research on MPC solutions for solar (thermal) power plants are very complex and address other control objectives (Galvez-Carrillo et al., 2009; Andrade et al., 2013; Camacho and Gallego, 2013).

Although this article demonstrates a relatively straightforward application of the proposed MPC-approach, it must be noted that this approach is entirely *modular* and *can easily be extended* by other auxiliary sources and also by additional outputs with varying draw-off temperatures decreasing from the top. This is of special interest for multivalent heating systems that comprise at least two of the following sources: a ST system, a PV&grid powered heat pump, a district or biomass heating.

In contrast to Halvgaard et al. (2012) who presents a closed solution for a special system, the proposed MPC approach is entirely open. Assume the connection of a PV powered heat pump to the system in Fig. 2, the approach may be extended by simply adding an according element in the mini-simulation for the disturbance prediction, and the cost function must be tailored for one additional control variable. In general the elements of the mini-simulation could be abstract functions, even the suggested solar loop as part of the mini-simulation may be reduced to one simple linear system with two or three inputs and one output. These extensions are also possible for the heat demand prediction not covered in this article.

5.4. Practical aspects

Thinking on utilizing the suggested MPC approach in practice, a few aspects and assumptions from Section 3 must be reconsidered. Ad (iv) Practical weather predictions are not 100% accurate, but probability bounds from weather forecasts can be facilitated to adjust the cost function weights, e.g. in case of insecure forecast data for irradiance $w^{\dot{q}_{aux}}$ could be reduced, resulting in more auxiliary heating. Ad (v) In terms of load prediction the SH and the DHW must be taken into account. The former may be predicted

dependent on T_a only and the latter may be approximated assuming a bimodal Gaussian profile, Jordan and Vajen (2005) and Mack et al. (1998) provide a good starting point. This is expected to reduce the probability for occurrence of critical situations as for scenario III winter and thus reduce also the penalties. Ad (vi) The MPC operated auxiliary source was assumed to be continuously adjustable which might not be the case in practice. This requires the definition of a rule which transforms the continuous signal into an on/off signal. Ad (vii) The mean temperature for the auxiliary volume is generally not available, but research efforts exist (see Haller, 2010), to place an *average temperature sensor* in the auxiliary volume. Using a Kalman Filter in connection with two local sensors (one at the upper and one at the lower boundary of V_{aux}) would also allow for a good approximation of the average temperature in V_{aux}. The continuous alignment of the thermal models is an effective measure to strengthen the robustness, although this issue should be analysed separately.

6. Conclusion

A feasible weather data incorporating model predictive control (MPC) approach for controlling the auxiliary heating in a thermal combistorage of a combisystem was demonstrated.

Disturbance-prediction, i.e. the estimation of expected solar thermal (ST) induced energy flux into and inside the thermal storage, is the main feature of the MPC. The suggested disturbance prediction, utilizing a mini-simulation developed from first principles, proved to function very well to disable auxiliary heating in case of foresighted solar irradiance. The disturbances, which shift the model states, can also be seen as a surrogate for continuous model linearisation.

The characteristic behavior of the MPC strongly depends on its numerous cost function parameters. The suitable range for the weight which values the use of auxiliary power turned out to be 0, $\cdots$, 2.5, and the weight for adjusting the reference temperature value in the auxiliary volume was kept constant at 1.

Given the investigated ST system with the load profile, the MPC approach is viable to demonstrate its strength for the months March, April and October, i.e. months where relatively high irradiance meets an according SH energy demand. Simulation results for these months show an absolute maximum increase of the solar fraction (F_s) by approximately 4 pp or 5%

with respect to the base case control, without any penalties. The maximum decrease of the auxiliary energy demand is 44%.

Any stated improvements consider a penalty compensation, hence they are purely due to the MPC approach. The MPC approach is viable to increase the ST system efficiency through optimal scheduling of the auxiliary energy supply resulting in reduced storage losses, increased ST input and finally reduced auxiliary energy supply.

Assuming application of this control approach for a ST system with high load even in summer (e.g. for a pure DHW system for a multi family house), the found performance improvement for certain months is likely to hold for all summer months.

Future developments to improve the MPC will focus on a suitable SH and DHW demand prediction to be incorporated into disturbance-prediction, and further MPC parameter tuning (e.g increasing of P) to reduce the appearing penalties. With respect to practice, a solution to obtain the actual average temperature in the auxiliary volume and a reasonable interpretation of inaccurate irradiance forecasts, is required (compare Oldewurtel et al., 2012).

Acknowledgements

This work has been partially funded by the following Projects: "ProgReg – Prognostizierende Regelungen zur Effizienzsteigerung von Solaranlagen" (Austrian Climate and Energy Fund, proj.-no.829826); "MacSheep – New Materials and Control for a next generation of compact combined Solar and heat pump systems with boosted energetic and exergetic performance" (EU's Seventh Framework Programme (FP7/2007-2013), grant agreement no. 282825).

Figure Captions

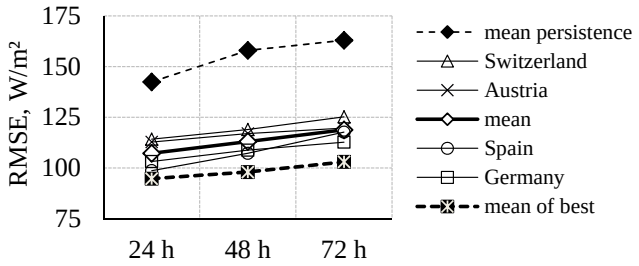

Figure 1: Annual RMSE for prediction of solar irradiance on the horizontal, in Europe, for three horizons; (data: Lorenz et al., 2009; Traunmueller and Steinmaurer, 2010), (for the US see Perez et al., 2011).

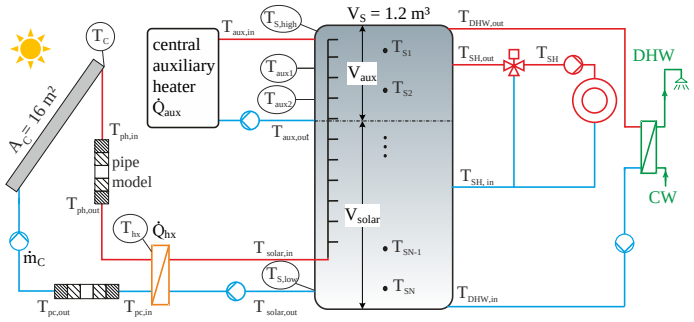

Figure 2: System hydraulics of the solar thermal combisystem, drawn with base case auxiliary control; $\dot{Q}_{aux}$ is controlled by the MPC for testing the suggested MPC approach.

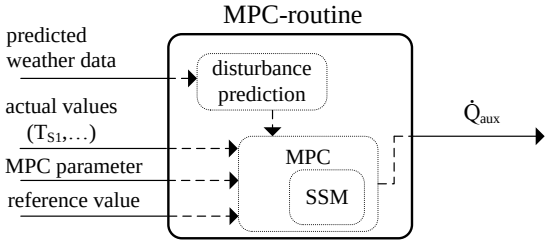

Figure 3: Overview of MPC-routine with essential inputs and the output. Disturbance-prediction means the transformation of expected solar radiation data, to resulting energy flux into and inside the storage. SSM indicates the storage model used by the MPC.

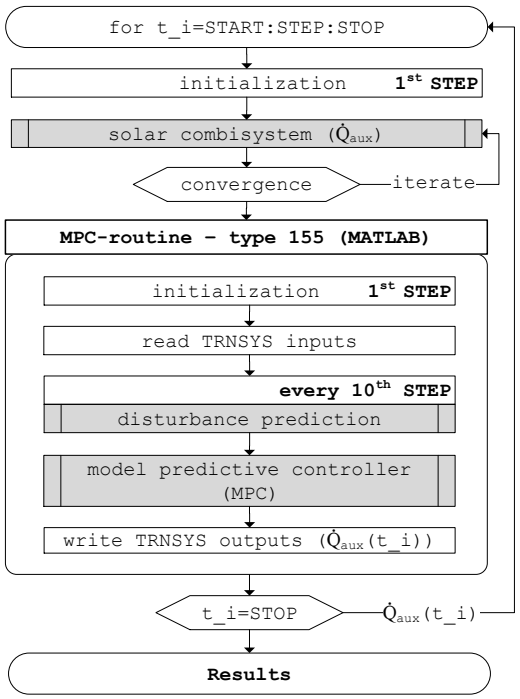

Figure 4: TRNSYS simulation flow chart for the MPC controlled ST system; for the base case $\dot{Q}_{aux}$ is either $\dot{Q}_{aux,max}$ or zero and the MPC routine is ignored.

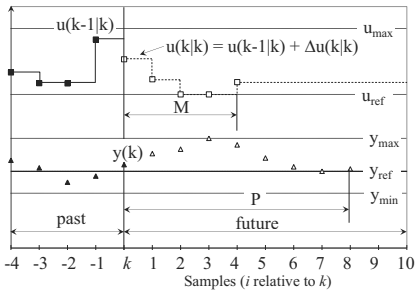

Figure 5: Exemplification of controller action (u) and controlled variable (y) for a MPC control scheme. P is the prediction horizon and M the control horizon in samples. The time between two samples is t_s; at instant k the variable $i = 0$.

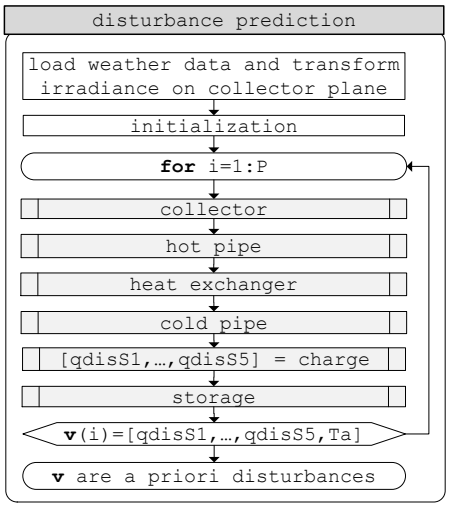

Figure 6: Generation of expected disturbances $\mathbf{v}$ for the thermal storage (SSM), given the actual time, the prediction horizon P and ideal weather forecast data.

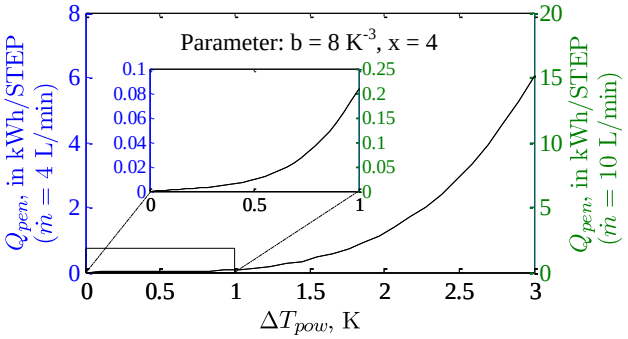

Figure 7: Penalty in kWh per simulation time STEP as a function of $\Delta T_{pow} \equiv \Delta T_{lin}$ for $T_{set} = 45$ °C which is assumed for this graph. Left axis is for low and right axis for high mass flow rate.

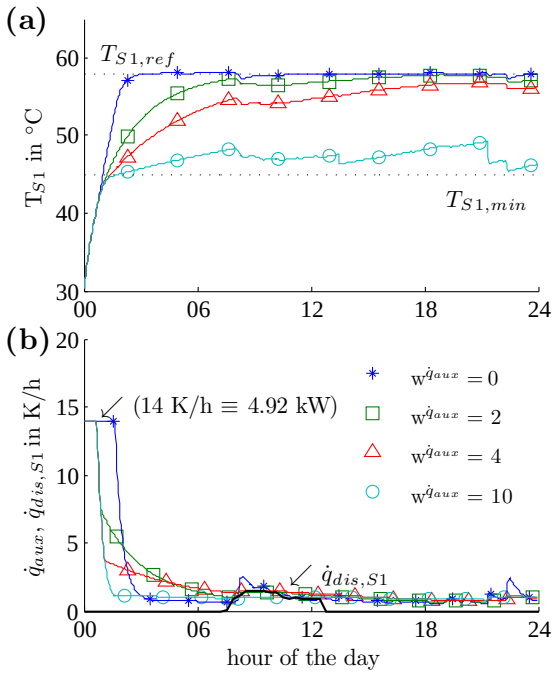

Figure 8: Scenario I; top storage temperature (a) and controller output (b) for four auxiliary power weights, which value the auxiliary energy demand in the cost function. Forecast: overcast ($I_{C,max} \approx 170$ W/m^2), pure DHW load, P = 12 h.

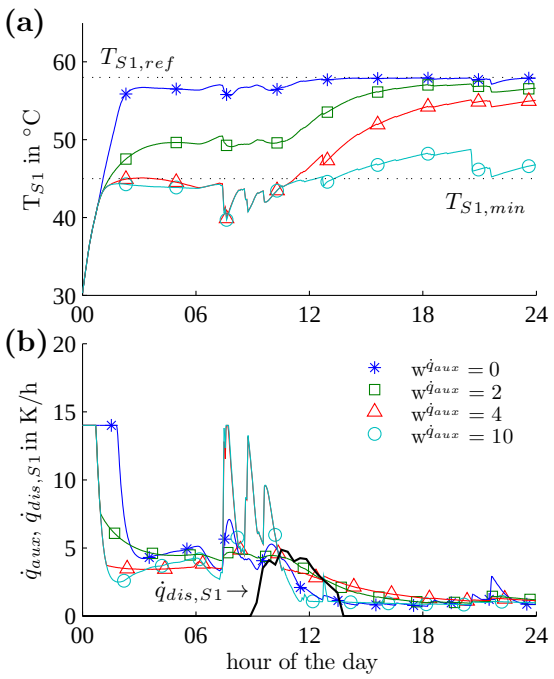

Figure 9: Scenario II winter; top storage temperature (a), and controller output and disturbance for the top node (b), for four auxiliary power weights. Forecast: partly cloudy ($I_{C,max} \approx 400$ W/m^2), DHW and SH load, P = 12 h.

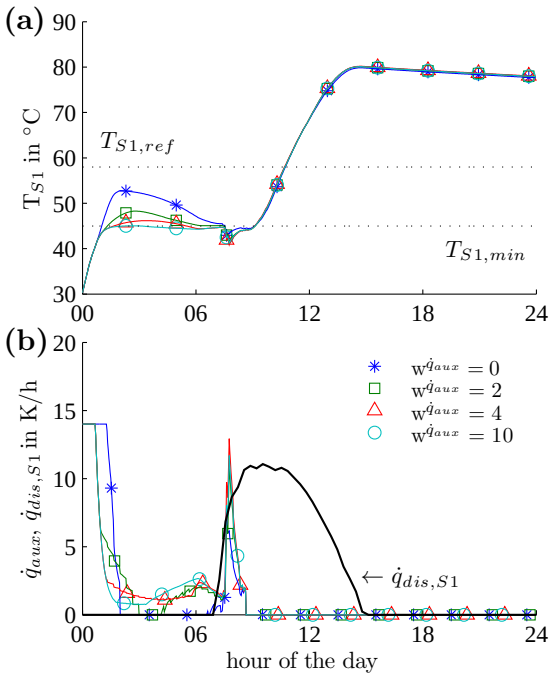

Figure 10: Scenario III winter; top storage temperature (a), and controller output and disturbance for the top node (b), for four different auxiliary power weights. Forecast: sunny ($I_{C,max} \approx 1000$ W/m^2), DHW and SH load, P = 12 h.

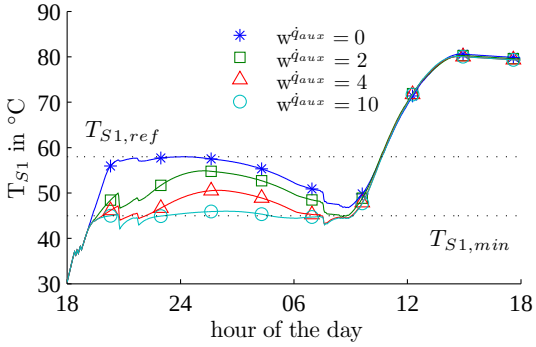

Figure 11: Scenario IV-P12; top storage temperature for four auxiliary power weights. Forecast: sunny ($I_{C,max} \approx 1000$ W/m^2), DHW and SH load, short prediction horizon: P = 12 h.

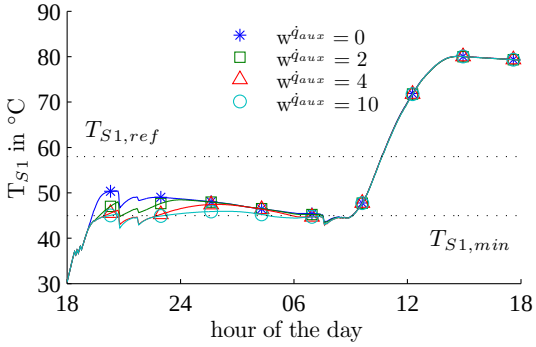

Figure 12: Scenario IV-P24; same as Fig. 11 but with longer prediction horizon: P = 24 h.

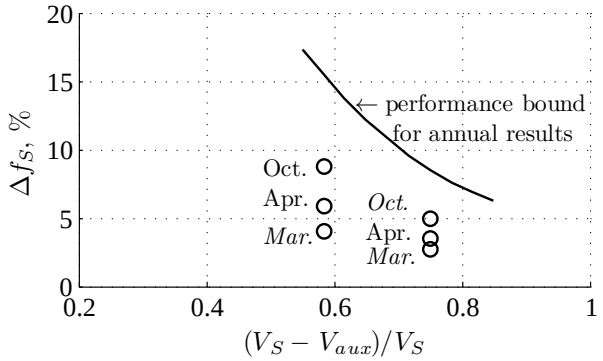

Figure 13: Performance change for increasing relative solar volume. The solid line indicates the theoretical performance bound (see Pichler et al., 2012); circles provide results for investigated months, for an *italic month* the penalties are significant.

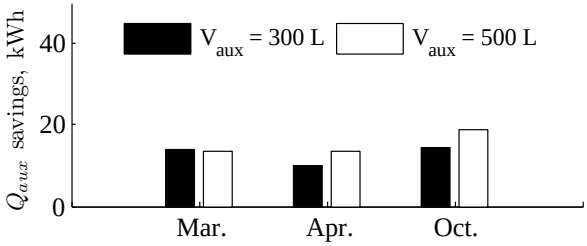

Figure 14: Reduction of auxiliary Energy demand for MPC operation; linear penalties were used to compensate missing auxiliary energy consumption.

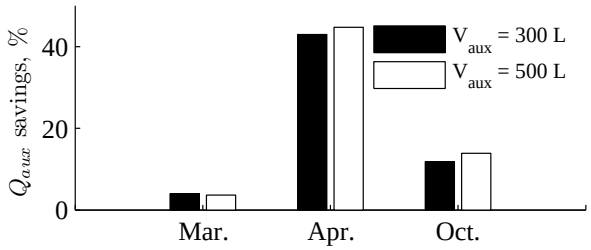

Figure 15: Reduction of auxiliary Energy demand for MPC operation (see Fig. 14) but in % with respect to the auxiliary energy demand of the base case for the according month.

Tables

Table 1: Nomenclature 1. Table

b, c	constants
A	area, m^2
c_p	specific heat capacity, J/kg K
$C_{min/max}$	min/max fluid heat capacity rate, J/h K
DHW	domestic hot water
F_s	solar fractions, %
I_C	global irradiance on the collector plane, W/m^2
L	length, m
$\dot{m}$	mass flow rate, kg/h
MPC	model predictive control/controller
N	upper bound of summation, –
NTU	number of transfer units
PT1	low pass first order
Q	thermal energy, J
$\dot{q}$	normalized thermal power, K/h
$\dot{Q}$	thermal power, W
QP	quadratic programming
RMSE	root-mean-square-error
RE	renewable energy
SFH	single family house
SH	space heating
SSM	state space model
ST	solar thermal
START	TRNSYS simulation start time, h
STEP	TRNSYS simulation time step, h
STOP	TRNSYS simulation stop time, h
t_i	discrete time instant of simulation, h
T	Temperature, °C
TES	thermal energy storage,
UA	heat loss coefficient, W/K
V	volume, m^3
x	power constant, –

Table 2: Nomenclature 2. Table

Subscript and Superscripts	
$*$	predicted value
a	ambient
b	brine
bot	bottom (node) of the storage
act	actual value
alt	alternative
aux	auxiliary
c	cap, or conduction
C	collector (plane)
dis	disturbance
hx	heat exchanger
in	inlet
i, j, k	indices
lin	linear
n	node
pen	penalty
pc	pipe cold
pow	power
ph	pipe hot
out	outlet
ref	reference value
set	set value
top	top (node) of the storage
S	storage, storage node
z	refering to vertical direction

Greek	
Δ	referring to (T) difference, K
ϵ	heat exchanger effectiveness, –
η_C	mean collector efficiency, –
λ	thermal conductivity, W/mK

Table 3: Solar thermal combisystem device and default parameters for the system in Fig. 2, (compare Heimrath and Haller, 2007; Dott et al., 2012).

Device	**Parameters and values**
Collector	A_C = 16 m^2, tilt = 45° southwards
	η = 0.8, c_0 = 3.5 W/m^2K, c_1 = 0.015 W/m^2K^2
Storage[a,b]	V_S = 1.2 m^3, V_{aux} = 0.3 m^3 default, λ_z = 2 W/mK
	insulation: λ = 0.04 W/mK, d = 0.15 m, T_a= 15 °C
Solar loop	on if $T_C > T_{SN}$ + 5 K
	off if $T_{SN} > 90$ °C or $T_{S1} > 95$ °C or $T_C > 100$ °C
Aux. heating, base case: on if $T_{aux1} < 57$ °C , off if $T_{aux2} > 63$ °C	
$\dot{Q}_{aux}$	$\dot{Q}_{aux,max}$ = 4.92 kW

[a] λ_z, the vertical heat conductivity, determines internal mixing.

[b] T_a, the ambient temperature is chosen constant, 15 °C.

Table 4: Specification of physical model properties.

$c_{p,b}$	specific heat brine	3.82 kJ/kgK
c_p	specific heat water	4.19 kJ/kgK
L_{Sh}	storage height	1.75 m
m_n	mass of one node	239.52 kg
$\dot{m}_C$	collector specific mass flow rate	15 kg/hm^2
UA	internal mixing UA value [a]	6.68 W/K
$UA_{a,c}$	UA value of top/bottom node	3.87 W/K
$UA_{a,m}$	UA value of medium nodes	1.93 W/K
	overall UA value of the storage	13.53 W/K
V_{aux}	auxiliary volume	0.3 m^3
ρ_w	density water	998 kg/m^3
ρ_b	density brine	1016 kg/m^3

[a] This value is 1.75 times the UA from the simulation model.

Table 5: MPC parameters and variables, and MPC tuning parameters used; abbreviations of quantities arising by means of the SSM during the prediction are indicated by an asterisk.

Abbreviations general, physical		**Description**	**Default, Unit**	
P	–	prediction horizon: 36 samples ≡ 12 h		
M	–	control horizon: 15 samples ≡ 5 h		
t_s	–	sampling time for MPC	1/3	h
ρ_ϵ	–	weight for constraint violation	–	–
ϵ	–	slack variable	–	–
y_{ref}	$T_{S1,ref}$	top node T, reference value	58	°C
w^y	$w^{T_{S1}}$	reference value, weight	1	1/K
y	T^*_{S1}	top node T, actual value	–	°C
y_{min}	$T_{S1,min}$	top node T, minimum	45	°C
V^y_{min}	$V^{T_{S1}}_{min}$	relaxation constant of minimum	1	K
y_{max}	$T_{S1,max}$	top node T, maximum	90	°C
V^y_{max}	$V^{T_{S1}}_{max}$	relaxation constant of maximum	100	K
u_{ref}	$\dot{q}_{aux,ref}$	auxiliary power, reference value	0	K/h
w^u	$w^{\dot{q}_{aux}}$	reference value, weight	2	h/K
u	$\dot{q}^*_{aux}$	auxiliary power, actual value	–	K/h
u_{min}	$\dot{q}_{aux,min}$	auxiliary power, minimum	0	K/h
V^u_{min}	$V^{\dot{q}_{aux}}_{min}$	relaxation constant of minimum	0	K/h
u_{max}	$\dot{q}_{aux,max}$	auxiliary power, maximum	14	K/h
V^u_{max}	$V^{\dot{q}_{aux}}_{max}$	relaxation constant of maximum	0	K/h
Δu	$\Delta\dot{q}^*_{aux}$	auxiliary power, rate of change	$\pm\infty$	K/h
$\mathrm{w}^{\Delta u}$	$w^{\Delta\dot{q}_{aux}}$	ditto, rate of change, weight	0.1	h/K

Table 6: Results for $\Delta F_s = F_{s,mpc} - F_{s,base}$ when applying the MPC, in pp and in % with respect to $F_{s,base}$. *Italic numbers* indicate significant penalties. In brackets are values from an alternative solar fractions definition: $F_s = 1 - \sum(\dot{Q}_{aux,S1} + \dot{Q}_{pen,lin}) / \sum(\dot{Q}_{DHW} + \dot{Q}_{SH})$.

Month	V_{aux}	$F_{s,base}$	ΔF_s	
	L	%	pp	%
Mar	300	58.7 (49.1)	*1.2 (1.9)*	*2.1 (3.8)*
	500	56.0 (45.6)	*1.3 (2.0)*	*2.4 (4.3)*
Apr	300	94.3 (91.1)	2.4 (3.8)	2.6 (4.2)
	500	92.8 (88.7)	3.2 (5.0)	3.5 (5.7)
Oct	300	73.7 (64.5)	*2.7 (4.1)*	*3.7 (6.4)*
	500	70.5 (59.6)	3.6 (5.6)	5.1 (9.4)

Appendix A. SSM for five node storage

Given the same assumptions as for the three node storage model, and using the definitions from Section 3.1.1 equivalently for a five node storage, the continuous time SSM matrices read

$$\mathcal{A} = \frac{1}{m_n c_p} \cdot \begin{bmatrix} -UA - UA_{a,c} & UA & 0 & 0 & 0 \\ UA & -2UA - UA_{a,m} & UA & 0 & 0 \\ 0 & UA & -2UA - UA_{a,m} & UA & 0 \\ 0 & 0 & UA & -2UA - UA_{a,m} & UA \\ 0 & 0 & 0 & UA & -UA - UA_{a,c} \end{bmatrix}, \tag{A.1}$$

$$\mathcal{B}_u = \mathbf{1}^{5\times 5}, \tag{A.2}$$

$$\mathcal{B}_v = \begin{bmatrix} 1 & 0 & 0 & 0 & 0 & UA_{a,c}/m_n c_p \\ 0 & 1 & 0 & 0 & 0 & UA_{a,m}/m_n c_p \\ 0 & 0 & 1 & 0 & 0 & UA_{a,m}/m_n c_p \\ 0 & 0 & 0 & 1 & 0 & UA_{a,m}/m_n c_p \\ 0 & 0 & 0 & 0 & 1 & UA_{a,c}/m_n c_p \end{bmatrix}. \tag{A.3}$$

Discretization with the according sampling time leads to the matrices $\mathbf{A}$, $\mathbf{B}_u$, $\mathbf{B}_v$ from Eq. (1). The output matrix is

$$\mathcal{C} \equiv \mathbf{C} = [1\ 0\ 0\ 0\ 0]. \tag{A.4}$$

Appendix B. Mini-simulation – thermal models

Irradiance transformation

This is accomplished using the radiation processing scheme of TRNSYS type 15, tiltMode 5, which accounts for horizon brightening, circumsolar and isotropic diffuse radiation by empirically derived "reduced brightness coefficients"; for more details on this see Perez et al. (1988, 1990) or TRNSYS (2010).

Collector

The collector model is based on the efficiency curve, (see Duffie and Beckman, 2006; Kaltschmitt et al., 2007). The steady state behavior of a flat plate collector is described by

$$\eta = c_0 - c_1 \cdot \frac{\bar{T}_C - T_a}{I_C} - c_2 \cdot \frac{(\bar{T}_C - T_a)^2}{I_C} \qquad \text{(B.1)}$$
$$\text{where } \bar{T}_C = \frac{T_{C,in} + T_{C,out}}{2} .$$

The parameters c_0, c_1 and c_2 define the efficiency curve; I_C is the irradiance on the collector plane and T_a is the ambient temperature. The actual collector field power is given by

$$\dot{Q}_C = \eta \; A_C \; I_C \qquad \text{(B.2)}$$

with A_C being the aperture area. The change of the mean absorber temperature can readily be calculated establishing the energy balance and using $c_{C,eff} = 7$ kJ/m^{2}K, as the specific effective heat capacity of the ST collector

$$\frac{d\bar{T}_C}{dt} = \frac{\dot{Q}_C - \dot{m}_C \cdot c_{p,b} \cdot (T_{C,in} - T_{C,out})}{A_C \cdot c_{C,eff}}. \qquad \text{(B.3)}$$

Pipe

The hot and cold pipes are modeled with a plug flow approach. For each pipe five elements and no mixing is assumed. The deployed model is developed as SSM, the used mathematical formulae are the same as those used in TRNSYS for type 31 (see Klein et al., 2010, pg. 4-195).

Heat exchanger

The effectiveness-NTU method is used to model the heat exchanger. It has a major advantage compared to the log mean temperature difference method, because iterative calculations are not needed if only the input temperatures of e.g. a counter flow plate heat exchanger are given. Assume that the primary and the secondary capacity mass flow rate, and the respective input temperatures are given, and the overall heat transfer coefficient of the external heat exchanger as a function of the collector field size A_C is given according to Heimrath (2004) by

$$UA = 88.561 \cdot A_C + 328.19 \;\; in \;\; W/K, \qquad \text{(B.4)}$$

the effectiveness ϵ of a heat exchanger is defined as the ratio of the actual to the maximum possible heat transfer rate. For any heat exchanger

$$\epsilon = f\left(NTU, \frac{C_{min}}{C_{max}}\right) \quad \text{where} \quad NTU = \frac{UA}{C_{min}} \tag{B.5}$$

holds, and C_{min} and C_{max} are the minimum and maximum heat capacity flow rate. Given $\dot{Q}_{max} = f(C_{min}, C_{max}, T_{pri,in}, T_{sec,in})$ and ϵ, the primary and secondary outlet temperatures can be calculated. For more details we refer to Incropera and DeWitt (2002).

Stratification unit

The model *charge* stands for the process of stratified charging of the TES. It is determined by the secondary outlet temperature of the solar heat exchanger and a control function. This function chooses which node receives water from the heat exchanger. The charging process leads to a temperature increase in the respective node and in the nodes below. Duffie and Beckman (2006) describe stratified charging in more detail. Outputs of charge are essentially the a priori disturbances to be used by the MPC controller.

Thermal storage

The thermal storage plays an important role in the mini-simulation. It provides the inlet temperature for the secondary side of the heat exchanger, which is strongly correlated to the collector inlet temperature. The used model for the five-node storage is that described in Appendix A. Temperatures for the next time step k+1 are calculated according to Eq. (1) using $\mathbf{x}(k) = \mathbf{T}_S = [T_{S1}, \ldots, T_{S5}]^T$, $\mathbf{u}$(k)=0, and $\mathbf{v}(k) = [\dot{q}_{dis,S1}, \ldots, \dot{q}_{dis,SN}, 15]^T$.

References

Anadranistakis, M., Lagouvardos, K., Kotroni, V., Elefteriadis, H., 2004. Correcting temperature and humidity forecasts using Kalman filtering: potential for agricultural protection in Northern Greece. Atmospheric Research 71, 115 – 125.

Andrade, G., Pagano, D., Alvarez, J., Berenguel, M., 2013. A practical NMPC with robustness of stability applied to distributed solar power plants. Solar Energy 92, 106 – 122.

Augsten, E., 2012. FÃűrdern und Fordern. Sonne Wind & WÃďrme 3, 10–11.

Bacher, P., Madsen, H., Nielsen, H.A., 2009. Online short-term solar power forecasting. Solar Energy 83, 1772 – 1783.

Bales, C., DrÃijck, H., Jaehnig, D., Jordan, U., Kovacs, P., Letz, T., Peres, B., Streicher, W., Suter, J.M., Vajen, K., Visser, H., Weiss, W., 2003. Solar Heating Systems for Houses – a Design Handbook for Solar Combisystems. International Energy Agency. ISBN 1 902916 46 8.

BeigelbÃűck, B., 2009. AbschÃďtzung des Energieeinsparungspotentials durch Simulation einer Raumtemperaturregelung mit Hilfe von modellbasierten prÃďdiktiven Regelalgorithmen unter Verwendung einer idealen Wettervorhersage. Master's thesis. FH-Pinkafeld.

Bemporad, A., Morari, M., Ricker, N.L., 2010. Model Predictive Control Toolbox 3.2, Manual.

Bianchi, M.A., 2006. Adaptive Modellbasierte PrÃďdiktive Regelung einer KleinwÃďrmepumpenanlage. Ph.D. thesis. EIDGENÃŰSSISCHE TECHNISCHE HOCHSCHULE ZÃIJRICH.

Camacho, E., Gallego, A., 2013. Optimal operation in solar trough plants: A case study. Solar Energy 95, 106 – 117.

Cebecauer, T., Perez, R., Suri, M., 2010. High Performance MSG Satellite Model for Operational solar Energy Applications. Technical Report. ASES – Proc. Solar.

Coffey, B., Haghighat, F., Morofsky, E., Kutrowski, E., 2010. A software framework for model predictive control with GenOpt. Energy and Buildings 42, 1084 – 1092.

Doeswijk, T.G., 2007. Reducing Prediction Uncertainty of Weather Controlled Systems. Ph.D. thesis. Wageningen Universiteit.

Dott, R., Haller, M.Y., Ruschenburg, J., Ochs, F., Bony, J., 2012. The Reference Framework for System Simulations of the IEA SHC Task 44 / HPP Annex 38 Part A: General Simulation Boundary Conditions; Part B: Buildings and Space Heat Load. Technical Report. IEA.

DrÃijck, H., 2006. Multiport Store – Model, Type 340 Version 1.99F. Technical Report. ITW-UniversitÃď t Stuttgart.

Duffie, J.A., Beckman, W.A., 2006. Solar Engineering of Thermal Processes. Wiley.

Ferhatbegovic, T., Zucker, G., Palensky, P., 2011. Model Based Predictive Control for a Solar-Thermal System, in: IEEE Africon Conference Proceedings.

Fernandez-Jimenez, L.A., Munoz-Jimenez, A., Falces, A., Mendoza-Villena, M., Garcia-Garrido, E., Lara-Santillan, P.M., Zorzano-Alba, E., Zorzano-Santamaria, P.J., 2012. Short-term power forecasting system for photovoltaic plants. Renewable Energy 44, 311 – 317.

Galvez-Carrillo, M., Keyser, R.D., Ionescu, C., 2009. Nonlinear predictive control with dead-time compensator: Application to a solar power plant. Solar Energy 83, 743 – 752.

GÃď hler, C., Gwerder, M., Lamon, R., TÃűdtli, J., 2007. Optimal Contol of Cogeneration Building Energy Systems, Proceedings of Clima 2007 WellBeing Indoors, REHVA.

Girodo, M., 2006. Solarstrahlungsvorhersage auf der Basis numerischer Wettermodelle. Ph.D. thesis. Carl von Ossietzky Universitaet Oldenburg.

GrÃijnenfelder, W.J., TÃűdtli, J., 1985. The Use of Weather predictions and dynamic programming in the control of solar domestic hot water systems, in: Melecon'85, Madrid , Spain.

Gyalistras, D., Gwerder, M., 2010. Use of Weather and Occupancy Forecasts for Optimal Building Climate Control (OptiControl): Two Years Progress Report. Technical Report. Terrestrial Systems Ecology ETH Zurich, Building Technologies Division, Siemens Switzerland Ltd., Zug, Switzerland.

Haller, Y., 2010. Combined Solar and Pellet Heating Systems – Improvement of Energy Efficiency by Advanced Heat Storage Techniques, Hydraulics, and Control. Ph.D. thesis. Graz University of Technology.

Halvgaard, R., Bacher, P., Perers, B., Andersen, E., Furbo, S., Jorgensen, J.B., Poulsen, N.K., Madsen, H., 2012. Model Predictive Control for a

Smart Solar Tank Based on Weather and Consumption Forecasts. Energy Procedia 30, 270 – 278.

Heimrath, R., 2004. Simulation, Optimierung und Vergleich solarthermischer Anlagen zur RaumwÃd'rmeversorgung fÃijr MehrfamilienhÃd'user. Ph.D. thesis. Graz University of Technology.

Heimrath, R., Haller, M., 2007. IEA SHC – Task 32, Subtask A, The Reference Heating System, the Template Solar System. Technical Report. Institute of Thermal Engineering, Graz University of Technology.

Herrmann, C., Candas, V., Hoeft, A., Garreaud, I., 1994. Humans under showers: Thermal sensitivity, thermoneutral sensations, and comfort estimates. Physiology & Behavior 56, 1003–1008.

Incropera, F., DeWitt, D.P., 2002. Fundamentals of Heat and Mass Transfer. Wiley.

Jordan, U., Vajen, K., 2005. DHWcalc: PROGRAM TO GENERATE DOMESTIC HOT WATER PROFILES WITH STATISTICAL MEANS FOR USER DEFINED CONDITIONS, in: Proc. ISES Solar World Congress, Orlando (US), 8.

Kaltschmitt, M., Streicher, W., Wiese, A., 2007. Renewable Energy — Technology, Economics and Environment. Springer.

de Keizer, C., 2012. Simulation-based long-term fault detection of solar thermal systems. Ph.D. thesis. Kassel University.

Klein, S., Beckman, W., Mitchell, J., Duffie, J., Duffie, N., Freeman, T., Mitchell, J., Braun, J., Evans, B., Kummer, J., Urban, R., Fiksel, A., Thornton, J., Blair, N., Williams, P., Bradley, D., McDowell, T., Kummert, M., Arias, D., Duffy, M., 2010. A TRaNsient SYstems Simulation Program – TRNSYS 17.00.0019, Manual. Solar Energy Laboratory, University of Wisconsin-Madison.

Krause, M., 2003. Optimierungskonzept fÃijr grosse solarintegrierte WÃd'rmeversorgungsanlagen,. Ph.D. thesis. University Kassel.

Lorenz, E., Heinemann, D., Wickramarathne, H., Beyer, H.G., Bofinger, S., 2007. Forecast of Ensemble Power Production by Grid-connected PV Systems, in: 20th European PV Conference Proceedings.

Lorenz, E., Remund, J., MÃijller, S.C., TraunmÃijller, W., Steinmaurer, G., Pozo, D., Ruiz-Arias, J.A., Fanego, V.L., Ramirez, L., Romeo, M.G., Kurz, C., Pomares, L.M., Guerrero, C.G., 2009. Benchmarking of Different Approaches to Forecast Solar Irradiance, in: 24th European PV Solar Energy Conference Proceedings.

Lukasse, L., van Maldegem, J., Dierkes, E., van der Voort, A.J., de Kramer-Cuppen, J., van der Kolk, G., 2009. Optimal control of indoor climate in agricultural storage facilities for potatoes and onions. Control Engineering Practice 17, 1044 – 1052.

Maciejowski, J.M., 2002. Predictive Control with Constraints. Pearson Education.

Mack, M., Schwenk, C., KÃűhler, S., 1998. Kollektoranlagen im GeschoÃ§wohnungsbau — eine Zwischenbilanz. Proceedings of 11. Internationales Sonnenforum, KÃűln, Germany .

Mathiesen, P., Kleissl, J., 2011. Evaluation of numerical weather prediction for intra-day solar forecasting in the continental United States. Solar Energy 85, 967 – 977.

Meteotest, 2009. Meteonorm 6.1.0.9, Global Meteorological Database for Engineers, Planners and Education, Software and Data on CD-ROM.

Morari, M., Lee, J.H., 1999. Model predictive control: past, present and future. Computers & Chemical Engineering 23, 667 – 682.

Oldewurtel, F., Parisio, A., Jones, C.N., Gyalistras, D., Gwerder, M., Stauch, V., Lehmann, B., Morari, M., 2012. Use of model predictive control and weather forecasts for energy efficient building climate control. Energy and Buildings 45, 15 – 27.

Perez, R., Beauharnois, M., Karl Hemker, J., Kivalov, S., Lorenz, E., Pelland, S., Schlemmer, J., Knowe, G.V., 2011. Evaluation of Numerical Weather Prediction – solar Irradiance Forecasts in the US. American Solar Energy Society – Proc. ASES Annual Conference, Raleigh, NC .

Perez, R., Ineichen, P., Seals, R., Michalsky, J., Stewart, R., 1990. Modeling daylight availability and irradiance components from direct and global irradiance. Solar Energy 44, 271–289.

Perez, R., Kivalov, S., Schlemmer, J., Jr., K.H., Renne, D., Hoff, T.E., 2010. Validation of short and medium term operational solar radiation forecasts in the US. Solar Energy 84, 2161 – 2172.

Perez, R., Moore, K., Wilcox, S., Renne, D., Zelenka, A., 2007. Forecasting solar radiation – Preliminary evaluation of an approach based upon the national forecast database. Solar Energy 81, 809 – 812.

Perez, R., Stewart, R., Seals, R., Guertin, T., 1988. The development and verification of the Perez diffuse radiation model. Technical Report. Sandia National Labs, State Univ. of New York, Atmospheric Sciences Research Center.

Pichler, M.F., DrÃűscher, A., Schranzhofer, H., aned G.I. Giannakis, G.K., Kosmatopoulos, E., Rovas, D., 2011. Simulation-Assisted Building Energy Performance Improvement Using Sensible Control Decisions. BuildSys'11 Proceedings, Seattle, WA, USA,.

Pichler, M.F., Lerch, W., Heinz, A., Heimrath, R., Schranzhofer, H., 2012. Auxiliary Energy Saving Potential of Solar Thermal Systems with predictive Controls, in: EuroSun Conference Proceedings, ISES.

Privaraa, S., Cigler, J., Zdenek, V., Oldewurtelb, F., Sagerschnigc, C., Eva, Z., 2013. Building modeling as a crucial part for building predictive control. Energy and Buildings 56, 8–22.

Richardson, D., Bidlot, J., Ferranti, L., Ghelli, A., Haiden, T., Hewson, T., Janousek, M., Prates, F., Vitart, F., 2011. Verification statistics and evaluations of ECMWF forecasts in 2010-2011. Technical Report. European Centre for Medium Range Weather Forecasts.

Rovas, D., 2011. PEBBLE Deliverable 3.2: PEBBLE Building Optimization and Control System. Technical Report. Technical University of Crete.

Schuss, M., 2011. Implementation of a predictive simulation-based controller for environmental systems in buildings. Ph.D. thesis. Vienna University of Technology.

Streicher, W., Bales, C., 2005. Combistores: Thermal energy storage for solar and low energy buildings, State of the art by the IEA Solar Heating and Cooling Task 32. University of Lleida, Spain.

Sturzenegger, D., Gyalistras, D., Morari, M., Smith, R.S., 2012. Semi-Automated Modular Modeling of Buildings for Model Predictive Control. Buildsys'12 Proceedings, Toronto, ON, Canada.

ThÃijr, A., 2007. Compact Solar Combisystem - High Efficiency by Minimizing Temperatures. Ph.D. thesis. Technical University of Denmark.

Traunmueller, W., Steinmaurer, G., 2010. Solar Irradiance Forecasting, Benchmarking of Different Techniques and Applications of Energy Meteorology, in: EuroSun Conference Proceedings, ISES.

Ullrich, S., 2013. Warme Grauzone. Erneuerbare Energien, Das Magazin 2.

Wang, X., Guo, P., Huang, X., 2011. A Review of Wind Power Forecasting Models. Energy Procedia 12, 770 – 778.

Wimmer, R.W., 2004. Regelung einer WÃd'rmepumpenanlage mit Model Predictive Control. Ph.D. thesis. ETH Zuerich.